Applied Physics Letters

RESEARCH ARTICLE | JUNE 26 2023

Pressure-induced ionic–polaronic–ionic transition in $LaAlO_3$

Special Collection: Accelerate Materials Discovery and Phenomena

Xingxing Zhao ; Jinqun Cai ; Dawei Jiang ; Min Cao ; Lin Zhao ; Yonghao Han

Appl. Phys. Lett. 122, 262101 (2023)
https://doi.org/10.1063/5.0155704

AIP Publishing

Applied Physics Letters ARTICLE pubs.aip.org/aip/apl

Pressure-induced ionic–polaronic–ionic transition in $LaAlO_3$

Cite as: Appl. Phys. Lett. **122**, 262101 (2023); doi: 10.1063/5.0155704
Submitted: 23 April 2023 · Accepted: 1 June 2023 ·
Published Online: 26 June 2023

Xingxing Zhao,[1] Jinqun Cai,[1,2] Dawei Jiang,[1] Min Cao,[1] Lin Zhao,[1,a)] and Yonghao Han[1,a)]

AFFILIATIONS

[1]State Key Laboratory of Superhard Materials, Institute of Physics, Jilin University, Changchun 130012, China
[2]International Center of Computational Method and Software, Jilin University, Changchun 130012, China

Note: This paper is part of the APL Special Collection on Accelerate Materials Discovery and Phenomena.
[a)]**Authors to whom correspondence should be addressed:** zhaolin_jlu@163.com and hanyh@jlu.edu.cn

ABSTRACT

Combining alternate-current impedance spectrum measurement and first-principle calculations, we thoroughly analyzed the electrical transport behavior of $LaAlO_3$ under high pressure. A pressure-induced ionic–polaronic–ionic transition has been discovered through impedance spectroscopy measurements. Through first-principle calculations, we have elucidated the physical origin of the emergence of polaronic conduction, which results from the distortion of electron density background around Al and O atoms. Furthermore, the discontinuous changes in the starting frequency of ion migration f_W, relaxation frequency f_b, and ionic resistance R_i have been found at around 13.2 GPa, which can be ascribed to the phase transition of $LaAlO_3$ from rhombohedral to cubic phase. Pressure can enhance the migration of O^{2-} ions, causing an increase in the ionic conductivity of $LaAlO_3$. This research will deepen our comprehension on the ion migration in solid electrolytes.

Perovskite lanthanum aluminate, $LaAlO_3$, has many advantages, such as low microwave losses,[1] high dielectric constant,[2–4] and excellent lattice matching with various high-temperature superconductors,[1,5,6] which makes it widely applied in microwave dielectrics, high-frequency ceramic capacitors, high-temperature superconducting thin film growth, and electrolytes for solid oxide fuel cells.[7–13] Previous studies have revealed that O^{2-} ion migration in $LaAlO_3$ plays a dominant role in affecting the electronic properties at oxide interfaces via causing large, nonlinear, and heterogenous polarizability of the lattice.[14] Moreover, oxygen vacancies play a vital role in oxygen ionic conduction and their concentration can be regulated by substituting ions with a different valence but of similar size.[15,16] By doping the A and B sites with different cations, a large number of oxygen vacancies are introduced into the structure, thus providing transport channels for oxygen ion migration and improving the ionic conductivity of $LaAlO_3$. For instance, Sr-doped $LaAlO_3$ ($La_{0.9}Sr_{0.1}AlO_{3-\delta}$) has been utilized as a solid electrolyte and exhibits a high ionic conductivity of $\sigma_i = 1.3 \times 10^{-2}$ S cm^{-1} at temperatures of about 900 °C.[17]

Pressure loading is an effective and clean physical approach for modifying the structure and electrical properties of materials without introducing chemical impurities.[18] For instance, pressure can induce the structural phase transition of $LiNbO_3$ from *R3c* to *Pnma* phase at 25.2 GPa and enhance the ionic conductivity.[19] $NaNbO_3$ undergoes a structural phase transition from *Pbcm* to $Pna2_1$ phase at 7.6 GPa, and meanwhile, ion channels become larger under high pressure, making ions transport easier.[20] Pressure-induced structural phase transition in $SrMoO_4$ from tetragonal to monoclinic phase at 7.0 GPa is also accompanied by an increase in ionic conductivity.[21] From the previous studies, it can be found that pressure has positive results in the enhancement of ionic conductivity of many ABO_3-type perovskite materials. For $LaAlO_3$, its applications in many aspects have relationships with its electrical properties. If pressure has the same positive effect on the enhancement of $LaAlO_3$ electrical properties, it will be of great significance for application.

So far, many studies have been conducted on the structure,[22,23] optical,[5,24–26] and elastic[27,28] properties of $LaAlO_3$ with various theoretical and experimental methods, such as first-principles calculations, *in situ* synchrotron radiation x-ray diffraction (XRD),[29–31] and Raman scattering measurements.[30] At high pressures, $LaAlO_3$ undergoes a structural transformation from a rhombohedral ($R\bar{3}c$) to a cubic ($Pm\bar{3}m$) phase at 14.8 GPa, with the AlO_6 octahedron recovering from its titled position to an ideal cubic perovskite structure without any tilting. However, systematic studies on the electrical properties of $LaAlO_3$ during compression, such as the behaviors of ion migration, polarization relaxation process, and dielectric response, have not been conducted. Therefore, further research in $LaAlO_3$ is expected to reveal phenomena under high pressure.

In this study, the influence of pressure on the dynamic behaviors of O^{2-} ion migration was analyzed by investigating the ionic transport characteristics of $LaAlO_3$ utilizing experimental and theoretical methodologies. We expect that this research will provide perspectives on how pressure affects O^{2-} ion migration in compression compounds and help us create solid electrolytes that can be utilized under extreme conditions.

The sample was commercially obtainable $LaAlO_3$ powder in purity of 99.9 % from Alfa Aesar Company. XRD refinement results showed that $LaAlO_3$ displays a rhombohedral structure with an $R\bar{3}c$ space group under environmental conditions (seen Fig. S5 in the supplementary material). In our high-pressure experiments, we used a diamond anvil cell (DAC) with anvil culet in diameter of 300 μm. A piece of pre-indented T-301 stainless steel in thickness of 60 μm was used as a gasket. A parallel-plate electrode configuration was adopted for alternate-current (AC) impedance measurement. The gasket and electrode were insulated by a mixture of alumina and epoxy powder. To avoid introducing extra impedance, we did not use pressure transmitting medium. The AC impedance spectra of $LaAlO_3$ were measured with Solartron 1260 impedance analyzer and 1296 interface. The frequency range for measuring the AC impedance spectroscopy was 10^{-3} to 10^{7} Hz, and the voltage amplitude was 1 V. High pressure was calibrated by the wave number of ruby fluorescence.[32]

First-principle calculations based on density functional theory (DFT) were performed within the generalized gradient approximation (Perdew–Burke–Ernzerhof functional).[33–38] To guarantee the convergence of enthalpy calculations, a suitable cutoff energy of 830 eV and Monkhorst–Pack k-point mesh-3×3×3 were selected. The valence states of the La, Al, and O atoms have the following electronic configurations: $5d^16s^2$, $3s^23p^1$, and $2s^22p^4$, respectively.

AC impedance spectroscopy is a valid approach to investigate the electrical transport behavior of charge carriers across the grain and grain boundary. In Figs. 1(a)–1(d), we displayed the Z' vs Z'' graphs of $LaAlO_3$ at different pressures. From ambient pressure to 3.5 GPa, $LaAlO_3$ has an ionic transporting profile, as demonstrated in Fig. 1(a), where a semi-circular arc appears in the high-frequency section and an upward-sloping straight line in the low-frequency section. The semicircle demonstrates the physical mechanism in which the O^{2-} ions vibrate at a very high frequency around their equilibrium positions within the lattice when a high-frequency alternate current signal is applied. Meanwhile, the sloping straight line denotes the long-range diffusion of O^{2-} ions as the alternate current signal becomes low. Notably, the slope of the inclined straight line deviates from $\pi/4$, which could be interpreted as an anisotropic transport of O^{2-} ions in the rhombohedral $LaAlO_3$.

From 3.5 to 5.7 GPa, the sloping straight line vanishes in the low-frequency range and only a semicircle is visible in impedance spectroscopy, as illustrated in Fig. 1(b). This implies that pressure restricts the initial movement of O^{2-} ions within the crystal lattice, causing the long-range diffusion of O^{2-} ions to disappear. An unusual ionic–electronic (or ionic–polaronic) transition induced by pressure occurs around 3.5–5.7 GPa.[39] However, it is uncertain whether the primary charge carriers are polarons or electrons. A thorough explanation is provided in the theoretical calculations section later in this paper.

When the pressure locates at 5.7 and 13.2 GPa, as represented in Fig. 1(c), the titled straight line starts to appear gradually in the low-frequency region, indicating that $LaAlO_3$ displays ionic conduction

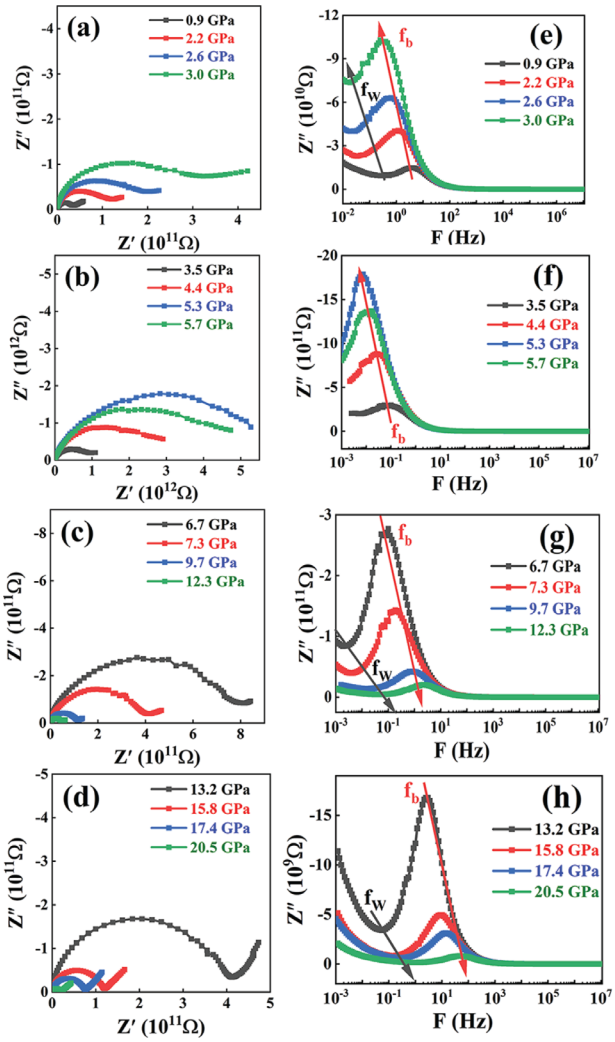

FIG. 1. (a)–(d) Nyquist representations. (e)–(h) Bode representations of the selected impedance spectra in $LaAlO_3$ at various pressures.

once more and O^{2-} ions long-range diffusion becomes more apparent as the pressure increases. The slope of the inclined straight line is still less than $\pi/4$, demonstrating that the conduction of O^{2-} ions is still anisotropic in the rhombohedral $LaAlO_3$.

As the pressure above 13.2 GPa, the slope of the inclined straight line in the low-frequency range becomes $\pi/4$, as illustrated in Fig. 1(d), which denotes that $LaAlO_3$ has typical ionic conduction, the conduction of O^{2-} ions increases significantly and is always isotropic in the cubic $LaAlO_3$. The slope variation of the titled straight line in the low-frequency area results from a pressure-induced structural phase transition from rhombohedral to cubic at 13.2 GPa.

Figures 1(e)–1(h) illustrate the frequency dependence of the imaginary impedance of $LaAlO_3$ at different pressures. By observing the changing trend of the imaginary impedance component in the low-frequency area, we can distinguish between ionic and electronic (or polaronic) conduction. Figures 1(e), 1(g), and 1(h) illustrate that

the imaginary impedance increases as the frequency decreases, exhibiting a typical ionic conduction mechanism. In contrast, the imaginary impedance decreases between 3.5 and 5.7 GPa with decreasing frequency, and the imaginary part does not tend to zero, as shown in Fig. 1(f), indicating the existence of polaronic or electronic conduction in $LaAlO_3$.

Given the discovery of the anomalous conduction transition sequence, we can qualitatively analyze the O^{2-} ions transport process of $LaAlO_3$ under high pressure by fitting the impedance spectra with suitable equivalent circuits. The representative equivalent circuits for ionic conduction and electronic (or polaronic) conduction fitting are displayed in Figs. 2(a)–2(c), respectively.

The electrical transportation mechanism in Figs. 2(a) and 2(c) is purely ionic conduction. Their impedance can be written in the following way:

$$Z = \frac{1}{\frac{1}{R_1 + Z_W} + \frac{1}{Z_{Q_1}}} + \frac{1}{\frac{1}{R_2} + \frac{1}{Z_{Q_2}}}, \tag{1}$$

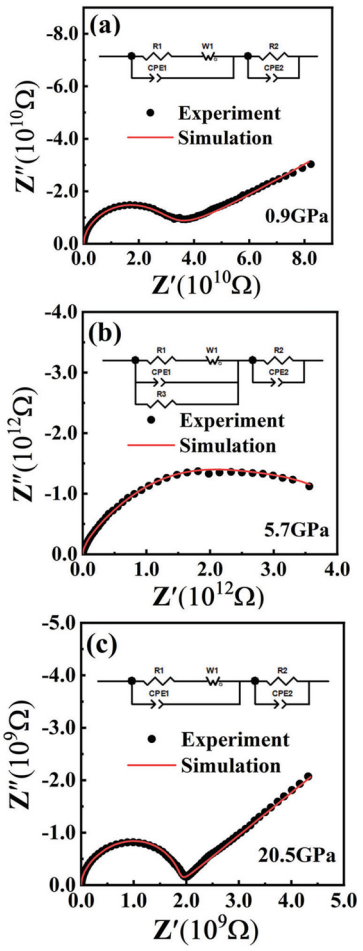

FIG. 2. (a)–(c) Selected fitting results and equivalent circuit diagrams of $LaAlO_3$ at 0.9, 5.7, and 20.5 GPa, respectively.

where R_1 and R_2 denote the resistances through the grain and grain boundary. The impedance of the Warburg equivalent element (Z_W) and constant phase element (Z_Q) can be expressed using the following equations:

$$Z_W = \sigma_W \omega^{-1/2}(1-j)\coth\left[\delta\frac{j\omega^{1/2}}{D}\right], \tag{2}$$

$$Z_Q = \sigma_Q (j\omega)^{-n}, \tag{3}$$

where σ_W and σ_Q stand for the Warburg and CPE coefficients, respectively, ω signifies the angular frequency ($\omega = 2\pi f$), D represents the O^{2-} ions diffusion coefficient, and δ denotes the average O^{2-} ions diffusion length. As the frequency decreases to zero, the imaginary part of the impedance tends to infinity, as illustrated in Figs. 1(e), 1(g), and 1(h), which is the characteristic of ionic conduction.

For electronic or polaronic conduction in Fig. 2(b), the impedance is represented by

$$Z = \frac{1}{\frac{1}{R_1 + Z_W} + \frac{1}{R_3} + \frac{1}{Z_{Q_1}}} + \frac{1}{\frac{1}{R_2} + \frac{1}{Z_{Q_2}}}, \tag{4}$$

where R_3 is the transferring resistance of polarons or electrons. These equivalent circuits can fit experimental results very well.

Based on the equivalent circuit analysis, the pressure-dependent starting frequency of ion migration f_W, relaxation frequency f_b, and ionic resistance R_i can be derived as shown in Fig. 3. In general, the frequency f_W at which the semicircle is connected to a straight line can be defined as the starting frequency of long-range O^{2-} ion migration. The higher f_W is, the faster O^{2-} ions migrates.[40] We can also see the change in f_W with pressure from the Z'' vs f plots in the black arrows of Figs. 1(e)–1(h). From ambient pressure to 3.5 GPa, f_W decreases apparently and shifts toward lower frequency as the pressure increases, which indicates that the diffusion of O^{2-} ions slows down under high pressure. On the contrary, when the pressure is above 5.7 GPa, f_W increases with increasing pressure, meaning that O^{2-} ions have fast

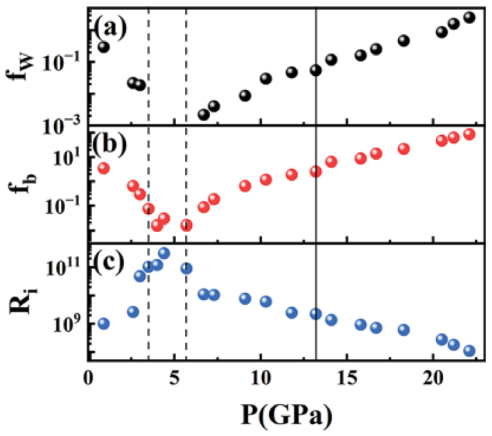

FIG. 3. The pressure-dependent (a) the starting frequency of ion migration f_W, (b) relaxation frequency f_b, and (c) ionic resistance R_i in $LaAlO_3$. The dotted lines show the pressure range of the experimentally discovered ionic–electronic (or ionic–polaronic) conduction mechanism, while the solid line denotes the phase change from rhombohedral to cubic at 13.2 GPa.

mobility under the electric field and can be diffused over a long range at higher frequencies. Thence, pressure enhances the diffusion of O^{2-} ions and improves the migration of $LaAlO_3$. As mentioned above, after 13.2 GPa, $LaAlO_3$ presents a standard ionic transport characteristic with a slope of $\pi/4$ for the inclined straight line, indicating the benefit isotropy of $LaAlO_3$. f_W increases abruptly with the pressure, increasing the diffusion rate of O^{2-} ions.

The relaxation frequency f_b, another parameter to describe the O^{2-} ions transport process, can be read out from the peak position of Z'' vs f plots as shown in Figs. 1(e)–1(h). The position of the relaxation peak characterizes the recovering speed of $LaAlO_3$ from a non-equilibrium to an equilibrium state under electrical field initiation. Figure 3(b) displays the f_b change with pressure. As the pressure increases from ambient pressure to 3.5 GPa, the relaxation frequency decreases, demonstrating that the migration rate of O^{2-} ions decreases with increasing pressure. As pressure increases from 3.5 to 5.7 GPa, the relaxation frequency f_b continues to decrease. Moreover, the relaxation peak is located between 10^{-1} and 10^{-2} Hz, which suggests the conduction of O^{2-} ions becomes more difficult. In contrast, between 5.7 and 13.2 GPa, the relaxation peak shifts to the high-frequency region with pressure increases, demonstrating that pressure can improve the O^{2-} ions diffusion. As the pressure reaches 13.2 GPa, the peak rapidly shifts to the high-frequency region with the pressure due to structural changes from the rhombohedral to the cubic phase.

From the pressure dependence of ionic resistance R_i as displayed in Fig. 3(c), it is evident that R_i changes in an opposite tendency with f_W and f_b, indicating R_i is in direct proportion to O^{2-} ion migration. In addition, from ambient pressure to 5.3 GPa, the ionic resistance R_i increases with the pressure and then decreases with increasing pressure after 5.3 GPa. This is because narrowing the bandgap causes a decrease in R_i. Moreover, the variation of the calculated bandgap with pressure is shown in Fig. S8.

To figure out the mechanism of O^{2-} ion migration under high pressure, especially the emergence of electronic conduction at high pressures between 3.5 and 5.7 GPa where the pressure-induced structural phase change is of absence, we conducted further theoretical calculations on the difference charge density of rhombohedral $LaAlO_3$ under high pressure.

Figure 4 illustrates the charge density difference of AlO_6 in $LaAlO_3$ at pressures of 0.0, 4.0, 5.0, and 13.0 GPa. There are two nonequivalent positions for O^{2-} ions in the AlO_6 octahedron, labeled O_I and O_{II} in Fig. 4. The central electron densities of O_I and O_{II} are listed in Table I. At ambient pressure, most electrons are concentrated around the O atoms, while only a few are near the Al atoms. Meanwhile, the number of electrons around O_I and O_{II} are similar (see Table I) and the O^{2-} ions can migrate in the lattice. It can be seen from the table that the electron density around O_{II} increases abruptly to 9.1×10^{-3} eÅ^{-3} at 5.0 GPa, which indicates that pressure increases the Coulomb interaction between O_{II} and Al ions and narrows the O^{2-} ion migration channels. Simultaneously, the local electronic background around Al atoms is distorted, further shielding the migration of O^{2-} ions and increasing ionic resistance. The shielding effects on O^{2-} ions and the local electron background distortion form polarons, meaning that polaronic conduction is the predominant process at 5.0 GPa. When the pressure reaches 13.0 GPa, the charge density around O_{II} decreases to 2.8×10^{-3} eÅ^{-3}, leading to the weak interaction between O_{II} and Al ions again and more free migration of O^{2-} ions. As the local background of electrons around

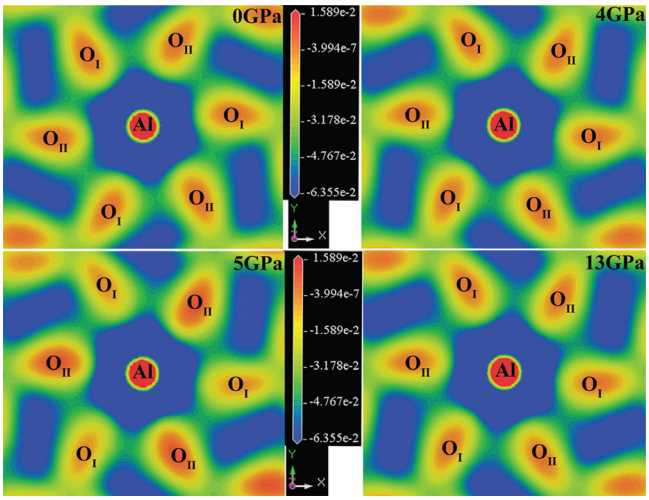

FIG. 4. The selected difference charge density in $LaAlO_3$ under high pressure.

TABLE I. The electron density of O_I and O_{II} at different pressures.

Pressure (GPa)	Electron density of O_I (10^{-3} eÅ^{-3})	Electron density of O_{II} (10^{-3} eÅ^{-3})
0	3.2	3.1
4	3.1	2.6
5	2.1	9.1
13	2.6	2.8

Al atoms gradually restores from the state of distortion, the polarons disappear and the conduction mechanism changes to ionic conduction under high pressure over 5.7 GPa. The theoretical calculation and experimental results are consistent.

In conclusion, we have conducted *in situ* impedance spectra measurements and first-principle calculations in $LaAlO_3$ under high pressure. Impedance spectra measurements have discovered an unusual ionic–polaronic–ionic transition induced by pressure. Using first-principle calculations, we have elucidated the physical origin of the emergence of polaronic conduction, which results from the distortion of electron density background around Al and O atoms. This study also shows that *in situ* impedance spectra measurements combined with first-principle calculations is a proper way to reveal the electrical transport properties of materials under high pressure. We hope these combined methods can be used in the future to discuss more issues about ion migration in solid electrolytes.

See the supplementary material for methods; molecular dynamics simulations; Rietveld refinement results of rhombohedral $LaAlO_3$; Z' and $\omega^{-1/2}$ plots; pressure-dependent R_g, R_{gb}, R_i, and R_e; and the variation of calculated bandgap with pressure.

This project was funded by the National Natural Science Foundation of China (Grant No. 11774126) and the National Key R&D Program of China (Grant No. 2018YFA0305900).

AUTHOR DECLARATIONS

Conflict of Interest

The authors have no conflicts to disclose.

Author Contributions

L. Zhao and Y. Han contributed equally to this work.

Xingxing Zhao: Conceptualization (equal); Formal analysis (equal); Investigation (equal); Methodology (equal); Visualization (equal); Writing – original draft (equal). **Jinqun Cai:** Formal analysis (equal); Methodology (equal); Software (equal); Writing – review & editing (equal). **Dawei Jiang:** Resources (equal). **Min Cao:** Investigation (equal). **Lin Zhao:** Conceptualization (equal); Software (equal). **Yonghao Han:** Conceptualization (equal); Funding acquisition (equal); Project administration (equal); Software (equal); Supervision (equal); Validation (equal); Writing – review & editing (equal).

DATA AVAILABILITY

The data that support the findings of this study are available from the corresponding authors upon reasonable request.

REFERENCES

[1]R. Brown, V. Pendrick, D. Kalokitis, and B. Chai, Appl. Phys. Lett. **57**, 1351 (1990).
[2]Y. G. Makeev, A. Motornenko, N. Cherpak, I. Babiichuk, and M. Kosmyna, Tech. Phys. Lett. **28**, 221 (2002).
[3]G. Samara, J. Appl. Phys. **68**, 4214 (1990).
[4]W. Xiang, H. Lü, L. Yan, H. Guo, L. Liu, Y. Zhou, G. Yang, J. Jiang, H. Cheng, and Z. Chen, J. Appl. Phys. **93**, 533 (2003).
[5]G. Murtaza and I. Ahmad, J. Appl. Phys. **111**, 123116 (2012).
[6]H.-F. Yu, J. Wang, S.-S. Wang, and Y.-M. Kuo, J. Phys. Chem. Solids **70**, 218 (2009).
[7]Q. Fu, F. Tietz, P. Lersch, and D. Stöver, Solid State Ion. **177**, 1059 (2006).
[8]C. A. da Silva and P. E. V. de Miranda, Int. J. Hydrogen Energy **40**, 10002 (2015).
[9]B. Chakoumakos, D. Schlom, M. Urbanik, and J. Luine, J. Appl. Phys. **83**, 1979 (1998).
[10]J. M. Phillips, J. Appl. Phys. **79**, 1829 (1996).
[11]C. Zuccaro, M. Winter, N. Klein, and K. Urban, J. Appl. Phys. **82**, 5695 (1997).
[12]J. Zylberberg and Z.-G. Ye, J. Appl. Phys. **100**, 086102 (2006).
[13]T. V. Raj, P. A. Hoskeri, H. Muralidhara, C. Manjunatha, K. Y. Kumar, and M. Raghu, J. Electroanal. Chem. **858**, 113830 (2020).
[14]J. Mannhart and D. G. Schlom, Science **327**, 1607 (2010).
[15]J. Sunarso, S. S. Hashim, N. Zhu, and W. Zhou, Prog. Energy Combust. Sci. **61**, 57 (2017).
[16]J. Sunarso, S. Baumann, J. Serra, W. Meulenberg, S. Liu, Y. Lin, and J. D. Da Costa, J. Membr. Sci. **320**, 13 (2008).
[17]T. L. Nguyen, M. Dokiya, S. Wang, H. Tagawa, and T. Hashimoto, Solid State Ion. **130**, 229 (2000).
[18]N. Reyren, S. Thiel, A. D. Caviglia, L. F. Kourkoutis, G. Hammerl, C. Richter, C. W. Schneider, T. Kopp, A.-S. Rüetschi, D. Jaccard, M. Gabay, D. A. Muller, J.-M. Triscone, and J. Mannhart, Science **317**, 1196 (2007).
[19]Q. Wang, C. Liu, Y. Gao, Y. Ma, Y. Han, and C. Gao, Appl. Phys. Lett. **106**, 132902 (2015).
[20]Q. Wang, D. Sang, H. Jiao, C. Liu, W. Wang, Y. Han, Y. Ma, and C. Gao, Appl. Phys. Lett. **111**, 152903 (2017a).
[21]T. Qin, Q. Wang, D. Yue, H. Liu, T. Ji, Y. Han, Y. Zheng, and C. Gao, J. Phys. Chem. C **124**, 17932 (2020).
[22]M. Benam, N. Abdoshahi, and M. M. Sarmazdeh, Physica B **446**, 32 (2014a).
[23]X. Xie, Y. Cheng, B. Xiao, and Y. Ohki, Jpn. J. Appl. Phys., Part 1 **51**, 041103 (2012).
[24]M. Yaseen, A. Ashfaq, A. Akhtar, R. Asghar, H. Ambreen, M. K. Butt, S. Noreen, S. Ur Rehman, S. Bibi, S. M. Ramay, and A. Murtaza, Mater. Res. Express **7**, 015907 (2020).
[25]J.-X. Shen, A. Schleife, A. Janotti, and C. G. Van de Walle, Phys. Rev. B **94**, 205203 (2016).
[26]M. Benam, N. Abdoshahi, and M. M. Sarmazdeh, Comput. Mater. Sci. **84**, 360 (2014b).
[27]A. Boudali, B. Amrani, M. Driss khodja, A. Abada, and K. Amara, Comput. Mater. Sci. **45**, 1068 (2009).
[28]X. Luo and B. Wang, J. Appl. Phys. **104**, 073518 (2008).
[29]M. Guennou, P. Bouvier, G. Garbarino, and J. Kreisel, J. Phys.: Condens. Matter **23**, 395401 (2011).
[30]P. Bouvier and J. Kreisel, J. Phys.: Condens. Matter **14**, 3981 (2002).
[31]J. Zhao, N. Ross, and R. Angel, J. Phys.: Condens. Matter **16**, 8763 (2004).
[32]H. Mao, J.-A. Xu, and P. Bell, J. Geophys. Res. **91**, 4673, https://doi.org/10.1029/JB091iB05p04673 (1986).
[33]J. P. Perdew, K. Burke, and M. Ernzerhof, Phys. Rev. Lett. **77**, 3865 (1996).
[34]P. E. Blöchl, Phys. Rev. B **50**, 17953 (1994).
[35]G. Kresse and D. Joubert, Phys. Rev. B **59**, 1758 (1999).
[36]M. Segall, P. J. Lindan, M. A. Probert, C. J. Pickard, P. J. Hasnip, S. Clark, and M. Payne, J. Phys.: Condens. Matter **14**, 2717 (2002).
[37]P. Hohenberg and W. Kohn, Phys. Rev. **136**, B864 (1964).
[38]W. Kohn and L. J. Sham, Phys. Rev. **140**, A1133 (1965).
[39]J. Wang, Y. Han, H. Liu, G. Zhang, C. Liu, and C. Gao, Phys. Chem. Chem. Phys. **20**, 7492 (2018).
[40]J. Wang, G. Zhang, H. Liu, Q. Wang, W. Shen, Y. Yan, C. Liu, Y. Han, and C. Gao, Appl. Phys. Lett. **111**, 031907 (2017b).